PCCP

Accepted Manuscript

ROYAL SOCIETY OF CHEMISTRY

www.rsc.org/pccp

Physical Chemistry Chemical Physics
CREATED USING THE RSC LaTeX PCCP ARTICLE TEMPLATE – SEE www.rsc.org/electronicfiles FOR DETAILS
ARTICLE TYPE www. rsc.org/xxxxxx | XXXXXXXX

Enzyme kinetics and transport in a system crowded by mobile macromolecules

Carlos Echeverria[abc] **and Raymond Kapral,**[*a]

Received Xth XXXXXXXXXX 20XX, Accepted Xth XXXXXXXXX 20XX
First published on the web Xth XXXXXXXXXX 200X
DOI: 10.1039/b000000x

The dynamics of an elastic network model for the enzyme 4-oxalocrotonate tautomerase is studied in a system crowded by mobile macromolecules, also modeled by elastic networks. The system includes a large number of solvent molecules, as well as substrate and product molecules which undergo catalytic reactions with this hexameric protein. The time evolution of the entire system takes place through a hybrid dynamics that combines molecular dynamics for solute species and multiparticle collision dynamics for the solvent. It is shown that crowding leads to subdiffusive dynamics for the protein, in accord with many studies of diffusion in crowded environments, and increases orientational relaxation times. The enzyme reaction kinetics is also modified by crowding. The effective Michaelis constant decreases with crowding volume fraction, and this decrease is attributed to excluded volume effects, which dominate over effects due to reduced substrate diffusion that would cause the Michaelis constant to increase.

1 Introduction

In order to fully understand the nature of transport and enzymatic kinetics in the cell, effects arising from molecular crowding must be taken into account. That the interior of the cell is a medium highly crowded by a diverse variety of macromolecular species has long been appreciated[1–6] and many studies have been carried out to elucidate the effects of crowding on transport properties such as diffusion, protein conformational changes and aggregation, as well as enzymatic reaction rates[7–19]. These studies have shown that factors such as excluded volume can lead to non-ideal behavior that changes the thermodynamic properties of the system, and interactions with crowding elements can alter kinetic properties and mechanisms of reactions. An intricate interplay of factors can contribute to the effects of crowding in a specific system so that the observed phenomena may differ from system to system.

In this paper we describe the results of simulations of the transport properties and reaction dynamics of an enzyme in an environment crowded by mobile macromolecules. Many models have been constructed and studied to explore such features.[20] Our system comprises an enzyme, substrate and product molecules, solvent, and macromolecules that act as crowding agents. All of the molecular species are treated at coarse-grained level of description and the entire system is evolved in time using an algorithm that combines molecular dynamics with a mesoscopic dynamical treatment of the solvent.[21,22] We consider an elastic network model[23] for a specific enzyme, the hexmeric enzyme 4-oxalocrotonate tautomerase (4-OT) that was constructed earlier[24]. It is composed of three dimers[25]; each monomeric enzyme in a dimer has 62 amino acid residues giving a total of 372 amino acid residues, which are represented by beads in our coarse-grain model. Each of the six active sites in the enzyme catalyzes the isomerization of unsaturated ketones[26]. This enzyme does not undergo substantial local or global conformational changes in the course of enzymatic catalysis.[27] The macromolecules that crowd the system are also modeled by elastic networks of beads. This particle-based description of all species in the system allows us to investigate in molecular detail the origins of the changes in protein transport properties and reaction kinetics for this system. We show how protein diffusion and orientational relaxation vary with the volume fraction ϕ of macromolecules, and how the kinetic constants that characterize the catalytic enzyme reactions change with ϕ.

The outline of the paper is as follows: Section 2 describes the model for the system in more detail as well as the method used to simulate the dynamics. The results of simulations of the diffusion and orientational relaxation of the protein as functions of the volume fraction of crowding macromolecules is presented in Sec. 3, while results pertaining to the modifications of enzyme kinetics by crowding are given in Sec. 4. The conclusions of the study are in Sec. 5.

[a] *Chemical Physics Theory Group, Department of Chemistry, University of Toronto, Toronto, ON M5S 3H6, Canada. E-mail: rkapral@chem.utoronto.ca; Fax: +1-416-9785325; Tel: +1-416-9786106*
[b] *CeSiMo, Facultad de Ingeniería. Universidad de Los Andes, Mérida 5101, Venezuela. E-mail: cecheve@ula.ve*
[c] *Department of Nanotechnology Engineering, Polytechnic University of Sinaloa, 82199 Mazatlan, SIN, Mexico*

2 Model for crowded enzymatic system

The model for the dynamics of a 4-OT enzyme carrying out catalytic conversion of substrate to product molecules in a crowded system was constructed as follows: The enzyme was modeled as an elastic network of beads whose equilibrium coordinates were taken to be the positions of the α-carbons of the constituent amino acids given in the literature[28]. Substrate, product and chemically inert solvent molecules were taken to be structureless particles. The substrate and product molecules interact with the enzyme and among themselves through intermolecular potentials, and the solvent molecules interact among themselves and with the other species by multiparticle collision (MPC) dynamics[21,22,29,30]. The 4-OT enzyme has six active sites, each of which catalyzes the conversion of substrate to product. An active site comprises a region defined by four beads and was constructed to model the structure of an active site of the real protein. Substrate molecules can bind to an active site through intermolecular potentials forming an enzyme-substrate complex; once bound they may dissociate to release substrate without reaction, or reaction to form product may take place. Thus, each active site undergoes catalytic reactions of the Michaelis-Menten (MM) type[31],

$$E + S \underset{k_{-1}}{\overset{k_1}{\rightleftharpoons}} C \xrightarrow{k_2} E + P, \tag{1}$$

where E, S, C and P denote the enzyme, substrate, enzyme-substrate complex and product, respectively. The full specification of the details of the intermolecular potentials and MPC dynamics have been given in an earlier study of the kinetics of this enzyme in bulk solution.[24]

The new feature in the present work is the presence of mobile polymeric obstacles that serve as crowding agents. As discussed above, the bead network model of the 4-OT enzyme was constructed from the experimentally determined coordinates of the α-carbons of the amino acids comprising the protein. In a cell the crowding elements are diverse in nature and include a variety of different proteins and biopolymeric filaments. Because of the complexity of the crowded cellular environment it is advantageous to focus on generic macromolecular crowding species instead of specific proteins or filaments. Although structureless spherical particles constitute perhaps the simplest way to model crowding species, we wished to incorporate some of the gross features associated with the irregular structures and diversity of shapes that real crowders exhibit. To this end we have chosen to adopt a highly coarse grained bead elastic network model for the obstacles. Even within this obstacle network description we make no attempt to model the full complexity of real macromolecular crowding species. Instead we consider species that are very roughly spherical in shape and, on average, have a characteristic radius, R_O. More specifically, to build an obstacle, its mean radius R_O and the number of obstacle beads N_O^b are first chosen. The positions of the N_O^b beads are drawn from a uniform distribution within a sphere of radius R_O. Since we do not wish to model any specific protein with a specific set of elastic network bonds, these beads are then simply connected globally by elastic springs to form a stiff but flexible network model of a generic protein. The total potential energy for an obstacle then takes the form,

$$V_{EN}^O(\mathbf{R}) = \sum_{n=1}^{n_L^O} \frac{1}{2} k |\mathbf{R}_n - \mathbf{R}_n^0|^2, \tag{2}$$

where $\mathbf{R}^0$ is collection of the initial random positions of the obstacle beads and n_L^O is the total number of bonds in the obstacle, with $n_L^O = N_O^b!/(2(N_O^b-2)!)$ for N_O^b obstacle beads. Finally, to place these obstacles in the system with a given volume fraction, a random position in the simulation volume is chosen from a uniform distribution and the center of mass of an obstacle is placed at that location. Other obstacles are similarly placed in the volume but accounting for volume exclusion of obstacles; if the obstacles overlap a new position is chosen for insertion. This process is continued until the desired volume fraction is obtained.

The interactions between beads in different obstacles, as well as the interactions of an obstacle bead with enzyme beads or substrate and product particles are described by repulsive Lennard-Jones potentials,

$$V_{LJ}(r) = 4\varepsilon \left[\left(\frac{\sigma_{OA}}{r} \right)^{12} - \left(\frac{\sigma_{OA}}{r} \right)^{6} + \left(\frac{1}{4} \right) \right] \theta(2^{1/6}\sigma_{OA} - r), \tag{3}$$

where $A = O, S$ and b for obstacle, substrate and enzyme beads, respectively, and $\theta(x)$ is the Heaviside function. An instantaneous configuration of the enzyme, obstacles, substrate and solvent molecules is displayed in Fig. 1. It shows the structures of the enzyme and obstacles as well as nature of the crowded medium in which the dynamics takes place.

This mesoscopic model for enzymatic dynamics in a crowded environment accounts for the structures of the enzyme and macromolecular mobile obstacles, reversible binding to the active sites of the enzyme to form the enzyme-substrate complex, and its subsequent dissociation to release product. In addition, chemically inert solvent molecules provide an environment in which these processes take place. The hybrid dynamics combines molecular dynamics of the solute species governed by intermolecular forces, with multiparticle collision dynamics for the solvent. This dynamics conserves mass, momentum and energy and, as a consequence, accounts for all hydrodynamic interactions among the constituents. These interactions are important for a correct description of transport and reaction kinetics in the condensed phase.

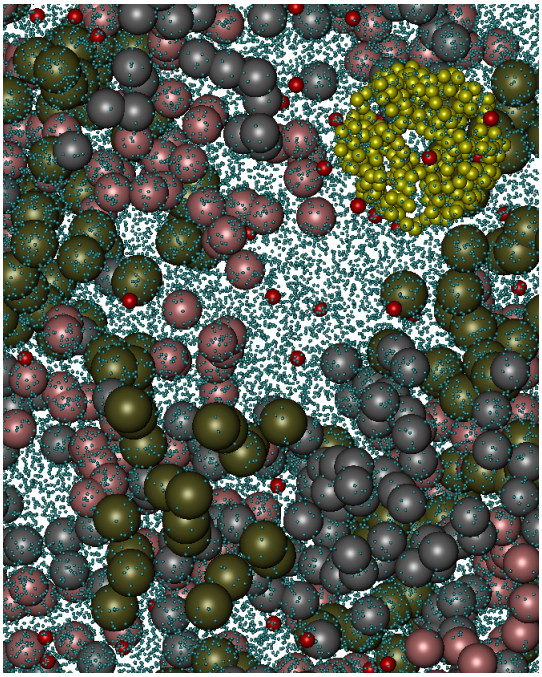

Fig. 1 An instantaneous configuration of the crowded enzymatic system. The elastic network models of the enzyme (yellow beads) and the obstacles (large colored beads; the color of each obstacle is used to distinguish the different obstacles) are shown. The substrates are rendered as red beads, while the chemically inert solvent particles are cyan colored points. The obstacle volume fraction is $\phi = 0.15$.

In the simulations of the dynamics of this system, we consider a single 4-OT enzyme in a cubic volume with sides $L = 30$ and periodic boundary conditions. This volume also contains substrate molecules with number density $[S_0] = n_S^0 = 0.01$, solvent molecules with density $n_0 = 11$, and obstacle macromolecules with volume fraction ϕ. Results are reported in dimensionless units.[32] In these units the diameter of an enzyme bead is $\sigma = 0.25$. The interaction energy between the two substrate molecules is characterized by $\varepsilon = 1$, while that for an enzyme bead and a substrate particle is $\varepsilon_{bS} = 10^{-6}$. The mass of a solvent molecule is $m = 1$ and the masses of protein and substrate beads are also taken to be $m_b = m_S = 1$. The other system parameters are: elastic network bond force constant, $k = 40$, and the reduced temperature $k_BT/\varepsilon = 5/12$. The reaction probabilities for unbinding substrate and forming product are $p_{-1} = 0.005$ and $p_2 = 0.005$. The MD time step is $\Delta t = 0.002$. The multiparticle collision time is $\tau = 0.1$.[33] The average radius of an obstacle is taken to be $R_O = 2.5$, which is comparable to $R_E = 2.2$, the mean radius of 4-OT. There are 372 amino acid beads in the 4-OT protein so the protein mass is $M = 372$. Given the generic manner in which the obstacles are treated there is no need to use a similar level of coarse graining for the obstacles. Instead we choose a much smaller number, $N_O^b = 20$, and assign the obstacle beads larger effective radii for their interactions. The mass of an obstacle bead is determined from $M_O^b = M_O/N_O^b = 20$, where $M_O = 400$ is the total mass of an obstacle. For the obstacles, $\sigma_{OO} = 2.0$, $\sigma_{OS} = 1.25$ and $\sigma_{Ob} = 1.25$. Typically results were computed from trajectories with length 25000, allowing for an equilibration period of 2500. Averages were obtained from many (1200) realizations of the dynamics.

3 Enzyme transport properties

It is well documented in both *in vivo* and *in vitro* experiments, as well as in simulation and theory, that enzyme diffusion often has a subdiffusive character in crowded or heterogeneous systems.[17,34–39] The subdiffusive character of the diffusive dynamics and the length of time over which it persists depends on whether the crowding elements are fixed in space or are mobile. For example, Monte Carlo simulations of two-dimensional systems crowded by mobile obstacles executing Brownian motion have shown that "protein" subdiffusive motion is transient and disappears at long time scales; however, if the obstacles are governed by Ornstein-Uhlenbeck noise the subdiffusive dynamics persists.[40]

The diffusive dynamics of the 4-OT enzyme in our crowded environment is also found to be subdiffusive. The mean square displacement (MSD) of the protein is $\Delta r(t)^2 = \langle |\mathbf{r}_{CM}(t) - \mathbf{r}_{CM}(0)|^2 \rangle$, where $\mathbf{r}_{CM}$ is the position of the center of mass of the protein and the angle brackets denote an average over time and different realizations of the dynamics. Figure 2 plots $\Delta r(t)^2/t$ on a double logarithmic scale for three values of the obstacle volume fraction ϕ, and compares these results with those for the enzyme in bulk solution in the absence of crowding elements.

Considering the protein in the absence of obstacles ($\phi = 0$), and assuming exponential decay of the autocorrelation function of the center-of-mass velocity, $C(t) = \frac{1}{3}\langle \mathbf{V}(t) \cdot \mathbf{V} \rangle = (k_BT/M)\exp(-t/\tau_v)$, the MSD of the protein is given by

$$\begin{aligned} \Delta r^2(t) &= 6\int_0^t \mathrm{d}t' \int_0^{t'} \mathrm{d}t'' \, C(t'') \\ &= 6Dt - 6\frac{k_BT}{M}\tau_v^2\left(1 - e^{-t/\tau_v}\right). \end{aligned} \tag{4}$$

The velocity relaxation time is $\tau_v = M/\zeta$, where ζ is the friction coefficient, which is related to the diffusion coefficient by the Einstein relation $D = k_BT/\zeta$. This expression describes the simulation data well with $\tau_v = 1.62$. (The fit is indistinguishable from the data in Fig. 2 on the scale of the figure.) The short time inertial regime predicted by this expression is evident in the figure. For long times the MSD takes the

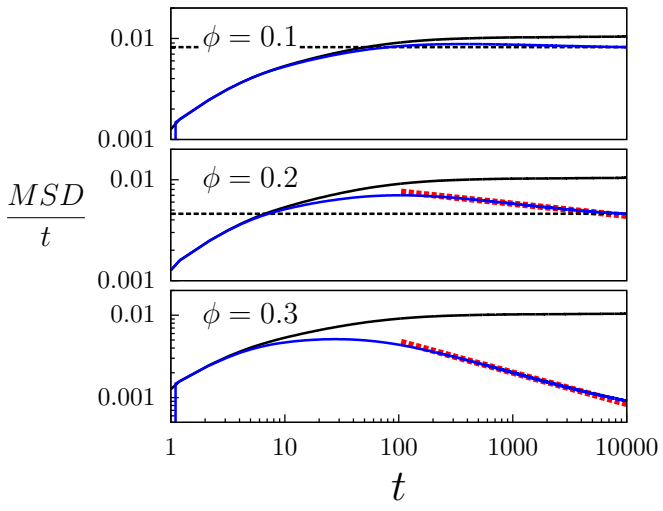

Fig. 2 Plots of the MSD divided by time as function of time t for several values of volume fraction ϕ: $\phi = 0$ (solid black lines), $\phi = 0.1$ (top), 0.2 (middle) and 0.3 (bottom) (solid blue lines), The dashed red lines are fits of $\Delta r(t)^2 = 6\Gamma t^\alpha$ to the simulation data, while the horizontal dashed black lines for $\phi = 0.1$ and 0.2 are guides to the eye that indicate the approximate asymptotic values.

usual form, $\Delta r(t)^2 = 6Dt$, with $D \approx 1.74 \times 10^{-3}$. For the large protein the friction coefficient should be well approximated by its Stokes law form, $\zeta = 6\pi\eta R_E$, where η is the solvent viscosity and $R_E = 2.2$ is the effective radius of the enzyme. The transport properties of the MPC solvent can be computed analytically[29,30] and the viscosity has the value $\eta = 6.128$ for our system parameters. Using these values, we find $\tau_\nu = 1.46$ and $D \approx 1.64 \times 10^{-3}$, which are comparable to the simulation values. Note that the diffusion coefficient of the large protein is much smaller than that of the small substrate molecules, $D_S = 0.048$, for the same system parameters. The substrate diffusion coefficient can also be computed analytically for MPC dynamics.[29,30] Identifying the effective radius of the 4-OT protein and its diffusion coefficient with those of the measured values of these quantities[41] allows us to establish a connection between our simulation units and physical units. This comparison yields $a \approx 1.3$ nm and $t_0 \approx 0.05$ ns.

Turning to finite obstacle volume fractions, we see clear deviations of the MSD from its value in bulk solution with increasing ϕ. Anomalous diffusion is characterized by a MSD of the form, $\Delta r(t)^2 = 6\Gamma t^\alpha$ with exponent $\alpha \neq 1$. The MSD plots show that after an initial rise in the inertial regime, there is an intermediate time period where $\Delta r(t)^2/t$ falls in accord with a power law $\Delta r(t)^2 = 6\Gamma t^{\alpha-1}$. For very long times the results suggest passage to a normal diffusive regime with lower values of the diffusion coefficients as a result of crowding; however, our finite-time simulations have not fully resolved this diffusive regime, especially for the largest volume fractions. Figure 3 gives the values of Γ (top) and α (bottom) as functions ϕ determined from double logarithmic fits to the intermediate time regime of $\Delta r(t)^2/t$. The exponent α decreases

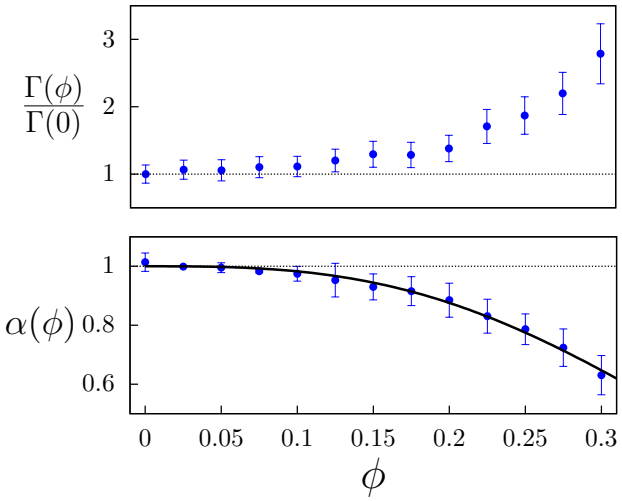

Fig. 3 Plots of the ratio $\Gamma(\phi)/\Gamma(0)$ (top panel) and α (bottom panel) versus ϕ. The black line is the fit of data for $\alpha(\phi)$ to the empirical equation, $\alpha(\phi) = \exp[-(\phi/\phi_\alpha)^\nu]$, with $\nu \approx 2.93$ and $\phi_\alpha \approx 0.398$. The error bars denote $\pm$ one standard deviation over 1200 realizations.

as ϕ increases, characteristic of a subdiffusive process, while the prefactor Γ increases with increasing ϕ. Previous Brownian dynamics simulations have shown that both crowding and hydrodynamic interactions contribute to the large reductions in the diffusion coefficients of macromolecules in the cell.[42] Our simulations account for hydrodynamic interactions and, in addition to crowding, these have a substantial effect on the diffusive dynamics.[27]

The orientational motion of the enzyme is also influenced by crowding. We define the orientational correlation function by $C_\theta(t) = \langle \hat{\mathbf{u}}(t) \cdot \hat{\mathbf{u}}(0) \rangle = \langle \cos\theta(t) \rangle$, where $\hat{\mathbf{u}}(t)$ is a unit vector from the center of mass of the protein to the center of mass of three of the active sites on one side of the protein. Figure 4 plots $C_\theta(t)$ for several values of the volume fraction. For $\phi = 0.0$, $C_\theta(t) \approx \exp(-t/\tau_c)$, with $\tau_R \approx 1397$. This value may be compared with that obtained from the Stokes-Einstein-Debye expression, $\tau_R^{(SED)} = 4\pi\eta R_E^3/k_BT$. Using the values of the enzyme radius, solvent viscosity and temperature given above, one finds $\tau_R^{(SED)} \approx 1968$. Since the enzyme is neither a solid object nor fully spherical only approximate agreement is expected and found. Figure 5, which plots the ratio $t_R(\phi)/t_R(0)$, shows how τ_R increases with the volume fraction. For these structured enzyme and obstacle macro-

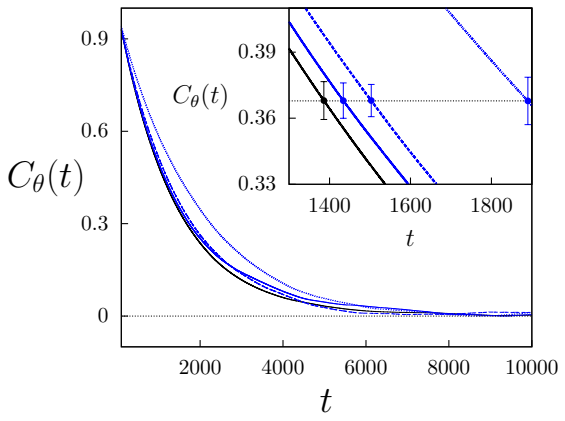

Fig. 4 Plot of $C_\theta(t)$ versus t for several values of the volume fraction: $\phi = 0.0$ (solid black line), $\phi = 0.1$ (solid blue line), $\phi = 0.2$ (dashed blue line) and $\phi = 0.3$ (blue points line). The inset shows the orientational relaxation times τ_R when $C_\theta(t)$ decays to $1/e$ of its initial value. The error bars were determined from 400 realizations of the dynamics.

molecules crowding hinders reorientation and is responsible for the observed substantial increase in τ_R with ϕ.

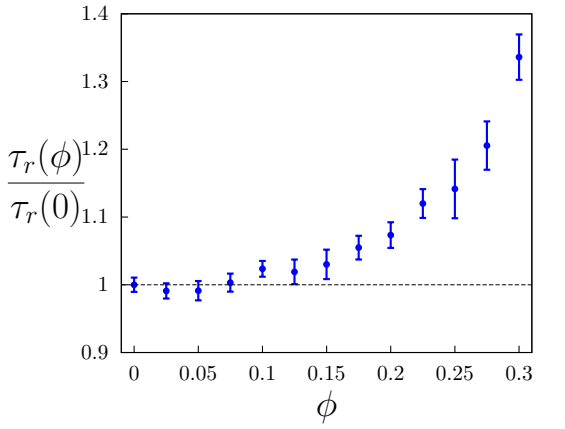

Fig. 5 Plot of the ratio $t_R(\phi)/t_R(0)$ versus ϕ for the protein. The error bars were determined from 400 realizations of the dynamics.

4 Enzymatic kinetics and crowding

The standard Michaelis-Menten model of enzymatic reactions is based on a mean field description of the chemical kinetics. In many circumstances this simple description is not sufficient since the assumption that diffusion is fast, so that the system remains well mixed at all times, may break down. In particular, diffusion can modify reaction rates and change the kinetics from reaction to diffusion control, and it can also give rise to power-law time dependence of rate coefficients. When such diffusion effects are taken into account the usual MM description of enzyme kinetics is modified.[43–45]

Molecular crowding can also alter enzyme catalysis and reduce the applicability of the MM mean-field picture. If the dynamics is subdiffusive, rate constants may exhibit power-law time dependence with exponents that depend on the volume fraction of crowding elements. This, in turn, can cause the temporal variations of chemical concentrations to differ from those of mean-field kinetics. The precise way that these effects manifest themselves depends on factors such as the nature and dynamical behavior of the obstacles (fixed or mobile) and the dimensionality of the system. Fractal Brownian motion, obstructed diffusion and various continuous-time random walk models have been constructed to investigate these reaction kinetic effects.[20,46,47]

Simulations and experiments have shown that the parameters that enter the MM description, such as the Michaelis constant K_M and the maximum velocity at which product is produced $v_{\max}$, can increase or decrease as function of the volume fraction depending on the specific characteristics of the enzyme and crowding molecules.[48–50] The results also show that not only is the volume fraction an important way to characterize crowding but the relative sizes of enzymes, substrates and crowding elements play important roles in determining the effects in some instances.[51] The changes in the relative magnitudes of factors such as excluded volume and reduced diffusion coefficients for different enzymes and crowding molecules can be responsible for the diverse results mentioned above. Thus, system-specific factors are likely to be responsible for how crowding changes enzyme kinetics.

Often discrete or continuous-time random walk models employing various noise sources and structureless fixed obstacles are used to study the effects of crowding on enzyme kinetics. Our particle-based dynamical model fully specifies the structures and interactions among the enzyme, substrate, product, solvent and crowding macromolecules. Thus, the type of diffusive dynamics, normal or subdiffusive, emerges naturally in the simulations, and we can explore in some detail the relative importance of the factors that may be responsible for changes in the reaction kinetics in this model system.

The enzymatic kinetics of 4-OT in bulk solution was studied earlier and compared to the MM model.[24] The activity of a single active site in the enzyme follows MM kinetics when there are no intermolecular interactions with protein beads that hinder full access to an active site. In this case the average number of enzyme-substrate complexes per active site in the system at time t is given by the standard MM expression,

$$\overline{N}_C(t) = \frac{[S_0]}{K_M + [S_0]} \left(1 - e^{-(k_1[S_0]+k_{-1}+k_2)t}\right), \qquad (5)$$

provided the substrate concentration does not change much from its initial value $[S_0]$ on the time scale of the evolution of $\overline{N}_C(t)$ to its quasi-steady-state value, $(\overline{N}_C)_{ss} = [S_0]/(K_M + [S_0])$. The Michaelis constant is $K_M = (k_{-1} + k_2)/k_1$. When all six active sites in the enzyme catalyze reactions, both interactions and correlations among the activities of these sites lead to quantitative deviations from MM behavior, even in the absence of crowding.[24] Nevertheless, the qualitative structures of the $\overline{N}_C(t)$ curves resemble those of MM kinetics, and it is useful to analyze our simulation results in this context since it provides some insight into the effects of crowding. In particular we focus on the Michaelis constant since many experiments measure this quantity.

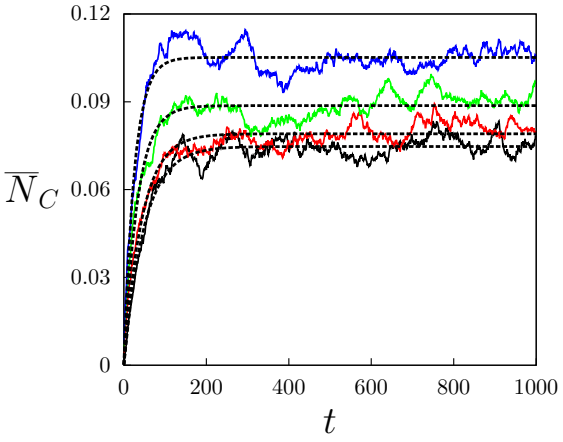

Fig. 6 The average number of enzyme-substrate complexes per active site $\overline{N}_C(t)$ versus time t for several values of the volume fraction: $\phi = 0.0$ (solid black line), 0.1 (solid red line), 0.2 (solid green line) and 0.3 (solid blue line). The dashed black lines are the fit of ec. (5) with simulation data. The results were computed from averages over 1200 realizations.

Figure 6 plots $\overline{N}_C(t)$ versus time for several values of ϕ. Note that the steady-state value, $(\overline{N}_C)_{ss}$, and the rise to this value increase with increasing volume fraction. This may be contrasted with the results for lattice models of fractal Brownian motion and obstructed diffusion with mobile obstacles which lead to slow kinetics.[47] Recall that the diffusive component of the dynamics that lead to binding of the substrate to the enzyme to form the enzyme-substrate complex depends on the sum of the substrate and enzyme diffusion coefficients. The substrates for 4-OT are small molecules, for example, 2-hydroxymuconate with a radius of a few Angstroms. The substrate size is much smaller than the enzyme and crowding macromolecules. Its diffusion coefficient is large and the effects of crowding will be small for volume fractions typically encountered in the cell. Similarly, our model substrate particles are small and their diffusion constant D_S is about two orders of magnitude larger than that of the enzyme, D. Since it is the substrate diffusion that dominates the diffusive kinetics leading to the formation of the complex, one might expect results that differ from those of larger substrate molecules that will exhibit more pronounced anomalous diffusion effects.

Using the simulation data for $(\overline{N}_C)_{ss}$, determined from the plots in Fig. 6, and assuming that the steady state value of the concentration of enzyme-substrate complexes per site is given by eq. (5), we may determine an effective Michaelis constant as a function of the volume fraction of obstacles. Figure 7 plots the values of $K_M(\phi)$ obtained in this way. One sees that for our model of the crowded 4-OT system K_M decreases with ϕ.

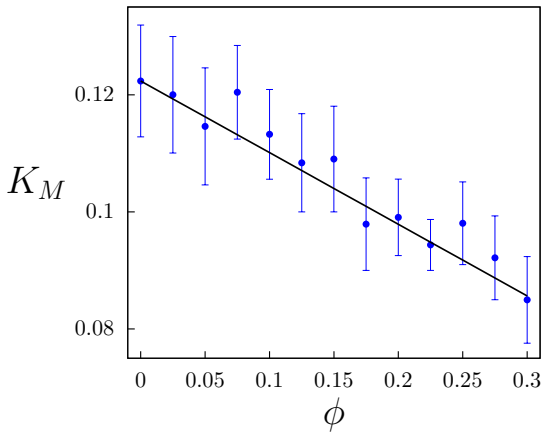

Fig. 7 Plot of the Michaelis constant $K_M(\phi)$ as a function of the volume fraction. The solid black line is corresponds to $K_M(\phi) = K_M(\phi = 0)(1 - \phi)$. The results were computed from averages over 1200 realizations.

For a system without obstacles, when diffusion effects are taken into account, the Michaelis constant has the form $K_M = K_M^0 + k_2/k_D$ where $K_M^0 = (k_{-1}^0 + k_2)/k_1^0$. This expression is obtained using the fact that the diffusion-influenced rate constants k_1 and k_{-1} have the forms[43] $k_1 = k_1^0 k_D/(k_1^0 + k_D)$ and $k_{-1} = k_{-1}^0 k_D/(k_1^0 + k_D)$. Here k_1^0 and k_{-1}^0 are the intrinsic values of k_1 and k_{-1}, respectively, assuming diffusion is very rapid, and $k_D = 4\pi D d_R$ is the Smoluchowski rate constant with D the relative diffusion coefficient of the enzyme and substrate and d_R is an effective radius for reaction at an active site. As noted earlier, since the substrate molecules are small compared to the enzyme $D \approx D_S$, where D_S is the substrate diffusion coefficient.

For our system D_S can be estimated analytically for MPC dynamics in the absence of obstacles and has the value $D_S = 0.048$. Direct simulation yields $D_S = 0.05$ in good agreement with this theoretical prediction. For the 4-OT enzyme $d_R = 0.5$

so that $k_D \approx 0.3$. The values of k^0_{-1} and k_2 are input parameters in our simulation and have the values $k^0_{-1} = k_2 = 0.005$. Also, k^0_1 can be estimated from the simulation data. The simulation value of K_M can be found from the steady state concentration of the enzyme-substrate complex. Given that all other quantities in $K_M = (k^0_{-1} + k_2)/k^0_1 + k_2/k_D$ are known, the value $k^0_1 = 0.09$ can be determined. The diffusion-influenced rate constants in the absence of crowding have the values, $k_1 = 0.07$ and $k_{-1} = 0.038$, and are dominated by reaction control. Crowding will decrease the diffusion coefficient and this, in turn, will lead to an increase in K_M, contrary to the simulation results. This suggests that reduced substrate diffusion is not the dominant factor in determining the volume fraction dependence of K_M.

The effects of crowding due to other enzymes on the rate coefficients in the MM model were investigated earlier.[45] In that study the enzymes were taken to be very simple structureless spherical particles. While simple, the dynamics accounted for the intermolecular interactions between the enzymes and substrate and product molecules, and included all hydrodynamic interactions that give rise to the proper diffusion-influenced kinetics for a system crowded by many such enzymes.

The rate constants for the association-dissociation reactions, $E + S \rightleftharpoons C$, could be determined directly from the simulations by counting the forward and backward reactive events. From these events one could then compute the forward and backward reaction rates, $\mathscr{R}_f$ and $\mathscr{R}_r$, respectively, and equate them to their mass-action forms to extract the rate constants as $\mathscr{R}_f = k_1(\phi)[E][S]$ and $\mathscr{R}_r = k_{-1}(\phi)[C]$. The rate constant $k_1(\phi)$ determined in this way depends strongly on ϕ, while $k_{-1}(\phi) = k_{-1}$ does not depend noticeably on ϕ. The equilibrium constant for this reaction is defined in terms of the activities of the species and takes the form, $K_{eq} = \gamma_C k_1(\phi)/(\gamma_E \gamma_S k_{-1}(\phi))$, where γ is an activity coefficient and detailed balance was used to replace the ratio of equilibrium concentrations by the rate coefficient ratio. Since $\gamma_C = \gamma_E$ and $\gamma_S = 1/(1-\phi)$ for this model, we have $K_{eq} = k_1(\phi)(1-\phi)/k_{-1}$. Simulations show that $k_1(\phi)(1-\phi)$ is independent of ϕ. Thus, we can write $k_1(\phi) = k_1/(1-\phi)$, where k_1 is again the $\phi = 0$ value of $k_1(\phi)$.

Similar considerations can be applied to our more complex and realistic enzymatic system. While it is possible that crowding could change k_{-1} and k_2, these changes are expected to be very small since the enzyme is quite rigid and does not undergo large scale conformational changes either globally or locally in the active site regions. The substrate binding rate constant $k_1(\phi)$ will, however, be subject to the same excluded volume effects as discussed above. Using the expression for $k_1(\phi)$ given above, $K_M(\phi)$ takes the form,

$$K_M(\phi) = K_M(\phi = 0)(1-\phi). \quad (6)$$

This equation is plotted as the solid line in Fig. 7 and provides an excellent description of the simulation data. For our model crowded enzymatic system, these results suggest that the modifications to reaction kinetics due to crowding are dominated by excluded volume effects on substrate binding to form the enzyme-substrate complex, rather than by the decrease in substrate diffusion. These results are consistent with the expectation that substrate diffusion will dominate over enzyme diffusion in determining the biding kinetics of the substrate to the enzyme, and that for small substrate molecules their diffusion is not anomalous or only weakly anomalous. This latter result is also consistent with lattice simulations that show that the transport of small particles is less anomalous in the presence of mobile obstacles than when the obstacles are immobile.[52]

Additional information concerning the encounters of the substrate molecules with the active sites of the enzyme can be obtained from the probability distributions of the lengths of time, t_L, it takes a substrate that is released from an active site to return to the same site, $P_s(t_L)$, or any of the other five other active sites on the enzyme, $P_o(t_L)$. Histograms, $H(t_L)$, of these quantities are shown in Fig. 8 for two values of the volume fraction; the insets show plots on double logarithmic scales. Considering the data for returns to the same active site, for both $\phi = 0$ and $\phi = 0.3$ one sees a rapid short time decay, which is longer in the presence of obstacles. For long return times one observes power-law scaling, $P_s(t_L) \sim t_L^{-\beta}$ with $\beta = 3/2$ as expected for a random walk.[53–55] This is consistent with the expectation that the subdiffusive character of the small substrate particles in the presence of mobile obstacles, if at all present, is much weaker than that of the large protein.

The histograms corresponding to $P_o(t_L)$ also show similar behavior at short and long first passage times with the same $\beta = 3/2$ power-law behavior at long times. The intermediate time regime shows more structure and exhibits a small maximum followed by power-law decay for both values of the volume fraction. These features are likely due to the complex structure of the 4-OT protein with six active sites. When a substrate is released from a given active site, some of the other active sites to which it may bind lie on the opposite side of the protein. In addition, since there is a channel in the protein through which substrate can pass, the intermediate binding times will differ from those of systems with simple geometries. Long binding times will still be governed by diffusion in the medium so that power-law behavior like that of $P_o(t_L) \sim t_L^{-3/2}$ is expected and observed.

5 Conclusion

The dynamical model for a crowded enzymatic system presented and studied in this paper incorporates several features, a number of which are not often treated in simulation studies of crowding. Both the enzyme and crowding macromolecules

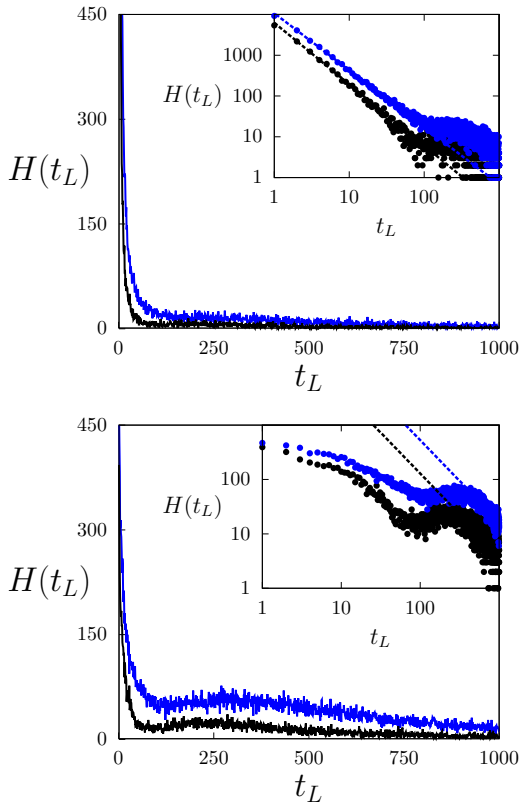

Fig. 8 Histograms of times t_L taken for a substrate released from an active site in the protein-substrate complex to rebind to same site (top panel) or a different site (bottom panel) for several values of volume fraction ϕ. The black points denote $\phi = 0$ and blue points denote $\phi = 0.3$. The dotted black lines in the insets correspond to fits to $t_L^{-3/2}$. The results were computed from averages over 1200 realizations.

are described at a coarse-grained level that models structural features of these molecules. The active sites in the protein are identified and binding, unbinding and reactive events are modeled explicitly. The enzyme, crowding macromolecules, substrate and product molecules interact through intermolecular potentials. Solvent is explicitly included. The dynamics preserves the important conservation laws of full molecular dynamics and, as a result, all hydrodynamic interaction in this complex system are automatically taken into account.

Because of this detailed description, insight into the molecular basis of crowding effects on transport and reaction kinetics can be obtained. In particular, for our model of the 4-OT enzyme, we found that crowding leads to a decrease of the effective Michaelis constant with increase in the volume fraction of crowding agents. This decrease is mainly determined by excluded volume effects on substrate binding to the enzyme, rather than by effects due to reduced substrate diffusion which would tend to increase K_M.

As in the experimental studies of various enzymatic systems, our results are system-specific. Since the 4-OT enzyme does not undergo large conformational changes in the course of reaction, its basic structure is not strongly influenced by the degree of crowding. This implies that the intrinsic rate constants will not change much due to crowding. This may not be the case for hinge proteins such as adenylate kinase or phosphoglycerate kinase which undergo large conformational changes during their catalytic cycles. The influence of crowding on the conformational structure of adenylate kinase has been studied and shown to have an effect.[56] A detailed mesoscopic model for the solution reaction kinetics of phosphoglycerate kinase has been constructed[57] and it would be interesting to examine its reaction kinetics under crowded conditions using the methods described here, since crowding could change the intrinsic reaction rates. Thus, simulation studies of the type described here could help resolve some of the issues related to the effects of molecular crowding on the biochemistry of the cell.

Acknowledgments

This work was supported in part by a grant from the Natural Sciences and Engineering Council of Canada. Computations were performed on the GPC supercomputer at the SciNet HPC Consortium, which is funded by the Canada Foundation for Innovation under the auspices of Compute Canada, the Government of Ontario, the Ontario Research Fund Research Excellence and the University of Toronto, and in part by the grant I-1370-13-02-B from Consejo de Desarrollo Cientifico, Humanístico y Tecnológico (CDCHT) of Universidad de Los Andes.

References

1 A. B. Fulton, *Cell*, 1982, **30**, 345.
2 D. S. Goodsell, *Trends Biochem. Sci.*, 1991, **16**, 203.
3 S. P. Zimmerman and A. P. Minton, *Annu. Rev. Biophys. Struct.*, 1993, **22**, 27.
4 T. C. Laurent, *Biophys. Chem.*, 1995, **57**, 7.
5 R. J. Ellis, *Trends Biochem. Sci.*, 2001, **26**, 597.
6 A. P. Minton, *J. Biol. Chem.*, 2001, **276**, 10577.
7 N. D. Gersohn, K. R. Porter and B. L. Trus, *Proc. Natl Acad. Sci. USA*, 1985, **82**, 5030.
8 K. Luby-Phelps, P. E. Castle, D. L. Taylor and F. Lanni, *Proc. Natl Acad. Sci. USA*, 1987, **84**, 4910.
9 A. S. Verkman, *Trends Biochem. Sci.*, 2002, **27**, 27.
10 M. Arrio-Dupont, G. Foucault, M. Vacher, P. F. Devaux and S. Cribier, *Biophys. J.*, 2000, **78**, 901.
11 T. Ando and J. Skolnick, *Proc. Natl Acad. Sci. USA*, 2010, **107**, 18457.
12 D. K. Eggers and J. S. Valentine, *Protein Sci.*, 2001, **10**, 250.
13 H.-X. Zhou, *J. Mol. Recognit.*, 2004, **17**, 368.

14 L. Stagg, S.-Q. Zhang, M. S. Cheung and P. Wittung-Stafshede, *Proc. Natl Acad. Sci. USA*, 2007, **104**, 18976.

15 S.-Q. Zhang and M. S. Cheung, *Nano Lett.*, 2007, **7**, 3438.

16 H.-X. Zhou, G. Rivas and A. P. Minton, *Annu. Rev. Biophys.*, 2008, **37**, 375.

17 F. Höfling and T. Franosch, *Rep.Prog. Phys.*, 2013, **76**, 046602.

18 S. Nakano, D. Miyoshi and N. Sugimoto, *Chem. Rev.*, 2014, **114**, 2733.

19 I. M. Kuznetsova, K. K. Turoverov and V. N. Uversky, *Int. J. Mol. Sci.*, 2014, **15**, 23090.

20 S. Schnell and T. E. Turner, *Biophys. Mol. Bio.*, 2004, **85**, 235.

21 A. Malevanets and R. Kapral, *J. Chem. Phys.*, 1999, **110**, 8605–8613.

22 A. Malevanets and R. Kapral, *J. Chem. Phys.*, 2000, **112**, 7260–7269.

23 M. M. Tirion, *Phys. Rev. Lett.*, 1996, **77**, 1905–1908.

24 C. Echeverria and R. Kapral, *Phys. Chem. Chem. Phys*, 2014, **16**, 6211–6216.

25 L. Chem, G. Kenyon, F. Curtin, S. Harayama, M. Bembenek, G. Hajipour and C. Whitman, *Biochemistry*, 1992, **267**, 17716.

26 C. P. Whitman, *Arch. Biochem. Biophys.*, 2002, **402**, 1.

27 The results of an investigation of the effects of crowding on the conformational dynamics of the hinge protein adenlyate kinase are given in C. Echeverria and R. Kapral, *Phys. Chem. Chem. Phys*, **14**, 6755 (2012).

28 See http://www.rcsb.org and A.B. Taylor and R.M. Czerwinski and W.H. Johnson Jr. and C.P. Whitman and M.L. Hackert, Biochemistry, **37**, 14692 (1998).

29 R. Kapral, *Adv. Chem. Phys.*, 2008, **140**, 89–146.

30 G. Gompper, T. Ihle, D. M. Kroll and R. G. Winkler, *Adv. Polym. Sci.*, 2009, **221**, 1–87.

31 L. Michaelis and M. L. Menten, *Biochem. Z.*, 1913, **49**, 333.

32 Lengths are measured in units of a, the cell size for multiparticle collisions, energy in units of ε and mass in units of m. The time unit is $t_0 = \sqrt{ma^2/\varepsilon}$.

33 The multiparticle collisions employed velocity rotations by angles $\pm\pi/2$ about randomly chosen axes. Grid shifting was used [T. Ihle and D. M. Kroll, Phys. Rev. E, **63**, 020201 (2001); ibid., **67**, 066705 (2003)].

34 S. Havlin and D. Ben-Avraham, *Adv. Phys.*, 1987, **36**, 695.

35 R. Metzler and J. Klafter, *Phys. Repts.*, 2000, **36339**, 1.

36 M. Wachsmuth, W. Waldemar and J. Langowski, *J. Mol. Biol.*, 2000, **298**, 677.

37 M. Weiss, M. Elsner, F. Kartberg and T. Nilsson, *Biophys. J.*, 2004, **87**, 3518.

38 D. S. Banks and C. Fradin, *Biophys. J.*, 2005, **89**, 2960.

39 G. Guigas, C. Kalla and M. Weiss, *Biophys. J.*, 2007, **93**, 316.

40 H. Berry and H. Chaté, *Phys. Rev. E*, 2014, **89**, 022708.

41 A. Taylor, R. Czerwinski, W. J. Jr., C. Whitman, M. H. J. T. Stivers, C. Abeygunawardana, C. P. Whitman and A. S. Mildvan, *Protein Science*, 1996, **5**, 729.

42 T. Ando and J. Skolnick, *Proc. Natl Acad. Sci. USA*, 2010, **107**, 18457–18462.

43 M. Eigen, W. Kruse, G. Maass and L. D. Maeyer, *Prog. Reac. Kinet.*, 1964, **2**, 287.

44 See, for instance, A. Szabo, J. Phys. Chem. **93**, 6929 (1989); N. Agmon and A. Szabo, J. Chem. Phys. **92**, 5270 (1990); H. Kim and K. J. Shin, Phys. Rev. Lett. **82**, 1578 (1999); G. Oshanin and O. Benichou and M. Coppey and M. Moreau, Phys. Rev. E, **66**, 060101(R) (2002); H. Kim and K. J. Shin, J. Phys: Condens. Matter **19**, 065137 (2007).

45 J.-X. Chen and R. Kapral, *J. Chem. Phys.*, 2011, **134**, 044503.

46 H. Berry, *Biophys. J.*, 2002, **83**, 1891.

47 M. Hellmann, D. W. Heermnn and M. Weiss, *EPL.*, 2012, **97**, 58004.

48 C. Balcells, I. Pastor, E. Vilaseca, S. Madurga and M. Cascante, *J. Phys. Chem. B*, 2014, **118**, 4062.

49 M. Norris and N. Malys, *Biochem Biophys.Res. Commun.*, 2011, **405**, 388.

50 L. Pitulice, I. Pastor, E. Vilaseca, S. Madurga, A. Isvoran, M. Cascante and F. Mas, *J. Biocatal Biotransformation*, 2013, **2**, 1.

51 C. Balcells, I. Pastor, , L. Pitulice, C. Hernandez, M. Via, J. L. Garces, S. Madurga, E. Vilaseca, A. Isvoran, M. Cascante and F. Mas, *New Front. Chem.*, 2015, **24**, 3.

52 A. Wedemeier, M. Merlitz and J. Langowski, *EPL*, 2009, **88**, 38004.

53 W. H. McCrea and F. J. Whipple, *Proc. Roy. Soc. Edinb.*, 1940, **60**, 281.

54 P. G. Doyle and J. L. Snell, *Random Walks and Electric Networks*, Mathematical Association of America, Washington, 1984.

55 I. M. Zaid, M. A. Lomholt and R. Metzler, *Biophys. J.*, 2009, **97**, 710.

56 C. Echeverria and R. Kapral, *Phys. Chem. Chem. Phys*, 2012, **14**, 6755–6763.

57 P. Inder, J. M. Schofield and R. Kapral, *J. Chem. Phys.*, 2012, **136**, 205101.